Acta Pharmaceutica Sinica B 2025;15(7):3756−3766

Chinese Pharmaceutical Association
Institute of Materia Medica, Chinese Academy of Medical Sciences

Acta Pharmaceutica Sinica B

www.elsevier.com/locate/apsb
www.sciencedirect.com

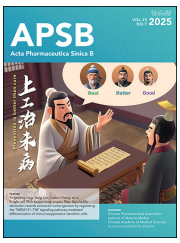

ORIGINAL ARTICLE

Engineered platelet-derived exosomal spheres for enhanced tumor penetration and extended circulation in melanoma immunotherapy

Jian Zhao[a,†], Xinyan Lv[c,†], Qi Lu[a], Kaiyuan Wang[a], Lili Du[a], Xiaoyuan Fan[a], Fei Sun[a], Fengxiang Liu[a], Zhonggui He[a], Hao Ye[b,*], Jin Sun[a,*]

[a]*Department of Pharmaceutics, Wuya College of Innovation, Shenyang Pharmaceutical University, Shenyang 110016, China*
[b]*Multi-Scale Robotics Lab (MSRL), Institute of Robotics & Intelligent Systems (IRIS), ETH Zurich, Zurich 8092, Switzerland*
[c]*School of Traditional Chinese Materia Medica, Shenyang Pharmaceutical University, Shenyang 110016, China*

Received 19 December 2024; received in revised form 6 March 2025; accepted 24 March 2025

KEY WORDS

Biological carrier systems;
Exosome spheres;
Phosphatidylserine;
CD47;
Prolong blood circulation time;
P-selectin;
Enhance adhesion;
Deep penetration

Abstract Cells and exosomes derived from them are extensively used as biological carrier systems. Cells demonstrate superior targeting specificity and prolonged circulation facilitated by their rich array of surface proteins, while exosomes, due to their small size, cross barriers and penetrate tumors efficiently. However, challenges remain, cells' large size restricts tissue penetration, and exosomes have limited targeting accuracy and short circulation times. To address these challenges, we developed a novel concept termed exosomal spheres. This approach involved incorporating platelet-derived exosomes shielded with phosphatidylserine (PS) and linked *via* pH-sensitive bonds for drug delivery applications. The study demonstrated that, compared with exosomes, the exosomal spheres improved blood circulation through the upregulation of CD47 expression and shielding of phosphatidylserine, thereby minimizing immune clearance. Moreover, the increased expression of P-selectin promoted adhesion to circulating tumor cells, thereby enhancing targeting efficiency. Upon reaching the tumor site, the hydrazone bonds of exosome spheres were protonated in the acidic tumor microenvironment, leading to disintegration into uniform-sized exosomes capable of deeper tumor penetration compared to platelets. These findings suggested that exosome spheres addressed the challenges and offered significant potential for efficient and precise drug delivery.

*Corresponding authors.
E-mail addresses: haoyeh@ethz.ch (Hao Ye), sunjin@syphu.edu.cn (Jin Sun).
†These authors made equal contributions to this work.

Peer review under the responsibility of Chinese Pharmaceutical Association and Institute of Materia Medica, Chinese Academy of Medical Sciences.

https://doi.org/10.1016/j.apsb.2025.04.013

1. Introduction

Immune checkpoint inhibitors (ICIs), an emerging class of immunotherapy agents, have revolutionized cancer treatment by enhancing survival rates[1-3]. However, the efficacy of ICIs is constrained in certain patients due to limited immunogenicity and intricate resistance mechanisms[4-8]. Chemotherapy can trigger immunogenic cell death, releasing tumor antigens and danger-associated molecular patterns (DAMPs) that activate immune pathways. Combined with ICIs can synergistically enhance immune responses and inhibit tumor progression. Nevertheless, achieving efficient delivery of chemotherapeutic agents to tumor sites remains a challenge[9-11].

Extensive research has been dedicated to investigating the potential of exosomes and cells as efficient carriers for drug delivery[12,13]. Exosomes overcome biological barriers with efficiency due to their small particle size, allowing them to penetrate tumor sites and deliver therapeutic agents[14-16]. Cells, on the other hand, exhibit superior targeting capabilities and prolonged circulation facilitated by their rich array of surface proteins. Despite these advancements, significant challenges persist in their development. Exosomes exhibit limited targeting precision and brief circulation durations in the bloodstream. Additionally, the larger size of cells restricts their capacity to traverse biological barriers and infiltrate tumor tissues[17,18].

To address these challenges, we developed an engineered exosome spheroid drug delivery system. Platelet-derived exosomes (Pex) expressing CD47 and P-selectin were isolated *via* ultracentrifugation and loaded with Doxorubicin (DOX) through co-incubation (PexD). To mask the apoptotic signal phosphatidylserine, we further co-incubated the exosomes with Annexin V (PPexD). Exosomes were assembled into spherical shapes using pH-sensitive MAL-PEOz-COOH (SPPexD). The maleimide group at one end of MAL-PEOz-COOH formed a stable thioether bond with the thiol group on the exosome surface, whereas the carboxyl group at the other end underwent condensation with the amino group on the exosome surface to form a peptide bond. The exosome spheres exhibited multiple advantages. In circulation, they shield PS and upregulated CD47 expression, evading macrophage clearance and extending blood circulation time[19,20]. Increased P-selectin expression facilitated adhesion to circulating tumor cells through CD44 recognition[21,22]. Upon reaching the tumor site, the acidic microenvironment protonated the hydrazone bonds linking the exosomes, causing them to break apart into uniformly sized single exosomes capable of deep tissue penetration. These single exosomes were then actively taken up by tumor cells, where the encapsulated DOX triggered immunogenic cell death, leading to DAMPs[23,24]. These DAMPs activated immune cells, such as T cells, triggering a robust anti-tumor immune response[25,26]. Compared with other treatment groups, the exosome-sphere group demonstrated the most pronounced anti-tumor efficacy. Finally, PD-L1 monoclonal antibody was combined with SPPexD to treat tumors. In summary, we have successfully constructed an efficient drug delivery platform with significant potential to improve drug delivery efficiency, inhibited tumor growth and distant metastasis, thereby providing a novel strategy for tumor treatment.

2. Materials and methods

2.1. Materials

DOX was obtained from Beijing Biolab Technology Co., Ltd. (Beijing, China). MAL-PEOz-COOH was sourced from Xi'an Ruixi Biotechnology (Xi'an, China). Annexin V was acquired from Beijing Dakowei Biotechnology (Beijing, China). 1,1′-Dioctadecyl-3,3,3′,3′-tetramethylindocarbocyanine iodide (DiR), Dulbecco's modified Eagle's medium (DMEM), fetal bovine serum (FBS), and 3-(4,5-dimethylthiazol-2-yl)-2,5-diphenyltetrazolium bromide (MTT) were purchased from Dalian Meilun Biotechnology (Dalian, China). Cell culture dishes were supplied by NEST Biotechnology (Wuxi, China). Hoechst 33342 and were provided by Beijing Solabo Technology (Beijing, China). The anti-PD-L1 antibody was obtained from Biolegend.

2.2. Methods

Fresh blood from mice (C57BL/6, 18−22 g, Shenyang Pharmaceutical University Animal Experiment Center) was centrifuged at 200×*g*, and the supernatant was suspended in an equal volume of ACD solution (citrate-dextrose) and then centrifuged at 800×*g*. To prepare Pex, platelets were diluted to 1×10^8 platelets/mL with HEPES buffer, combined with Ca^{2+} ionophore (10 mmol/L, Sigma−Aldrich) at 30 °C, incubated for 2 h, and then centrifuged at 800×*g* for 10 min. The collected supernatant was further ultracentrifuged, and the extracellular vesicles were ultracentrifuged at 100,000×*g* for 90 min to concentrate the particles. Resuspend the particles and filter through a 0.22 μm filter to obtain Pex. Pex was mixed with DOX in equal proportions in PBS and incubated at 37 °C for 1 h, followed by centrifugation at 100,000×*g* to remove free DOX to prepare PexD. PexD was incubated with Annexin V at 37 °C for 60 min to produce PPexD. PPexD was further incubated with MAL-PEOz-COOH on a shaker at 37 °C overnight. Finally, SPPexD was isolated by centrifugation at 10,000×*g*.

2.3. Western blot and SDS-PAGE analysis

Proteins extracted from platelets, Pex, PexD, PPexD, and SPPexD were heat-treated for 5 min and subsequently separated using SDS-PAGE gel electrophoresis. The proteins were then electrophoretically transferred to a Bio-Rad polyvinylidene fluoride membrane. These membranes were subsequently treated with a protein-blocking solution for 2 h before being exposed to antibodies specific for CD63 (Abcam), P-selectin (Abcam), CD47 (Abcam), and CD44 (Abcam) overnight at 4 °C. Then, diluted secondary antibody (1:10,000) was incubated with the samples for 2 h at room temperature.

2.4. Drug release in vitro

PexD, PPexD, and SPPexD were introduced into phosphate buffered saline (PBS) with a pH of 6.5 and 7.4 for dispersion and

maintained at ambient temperature. The release of DOX was measured at specified time intervals using a microplate reader set to a wavelength of 490 nm.

2.5. Study on antiphagocytosis and adhesion of SPPex

One million RAW264.7 macrophages and ten thousand B16-F10 melanoma cells were cultured overnight on a confocal dish at 37 °C. Subsequently, RAW264.7 macrophages were incubated with DiR-labeled particles, including Pex, PPex, platelets, and SPPex, at 37 °C for 1 h. Following this, the DiR-labeled vectors were co-incubated with B16-F10 cells at 4 °C for 1 h, after which the nuclei were stained using Hoechst 33342. Confocal laser scanning microscopy (CLSM) was then utilized to analyze the particles' adherence to tumor cells or engulfment by macrophages.

2.6. Cellular internalization study

B16-F10 cells were seeded into 24-well plates at a density of 5000 cells per well and cultured overnight. Following this, the cells encountered newly prepared media infused with various doses of DOX and were incubated at 37 °C for either half an hour or 2 h. The cellular uptake was evaluated by confocal laser scanning microscopy and FACS flow cytometry.

2.7. Cytotoxicity assays

B16-F10 cells were seeded in 96-well plates at a density of 1500 cells per well and cultured overnight. The cells were then treated with various agents and incubated for 24 h. Cytotoxicity was subsequently assessed by measuring absorbance at 570 nm using a microplate reader.

2.8. ICD induction by SPPexD

The various formulations were incubated with B16-F10 tumor cells in a 35-mm cell culture dish for 24 h. The supernatants were subsequently collected to measure HMGB1 and ATP levels, while calreticulin expression was analyzed *via* Western blotting. Immature dendritic cells (DCs), derived from mouse bone marrow, were then co-cultured with B16-F10 tumor cells pre-treated with the formulations. Dendritic cell maturation was evaluated using flow cytometry.

2.9. Tumor sphere penetration by SPPexD

B16-F10 cells were seeded at a density of 1×10^4 cells per well in 96-well plates with non-adherent bottoms. Aggregation was facilitated by centrifuging the plates at $1000 \times g$ for 3 min. Tumor spheroids, approximately 300 μm in size and exhibiting optimal density and evenness, were carefully chosen and relocated to dishes measuring 35 mm. They were incubated in DIR-labeled vector medium at 37 °C for 24 h. Visualization of drug distribution through the layers was achieved by employing a confocal microscope equipped with Z-stack scanning capability, progressing from exterior to interior strata.

2.10. In vivo elimination of circulating tumor cells (CTCs)

Evaluation of the SPPexD's ability to capture circulating tumor cells was conducted by first anesthetizing mice with isoflurane and then delivering different DOX formulations (40 μg) intravenously *via* the tail. A half-hour later,10 μL of saline containing 1×10^5 B16-F10 cells were also administered into the tail vein. After a period of two weeks from the injection, lung specimens were collected and subjected to staining and further analyzed through imaging techniques.

2.11. Biodistribution and pharmacokinetic study of SPPexD

A mouse model harboring the B16-F10 tumor was successfully created. Seven days later, mice ($n = 3$) received 1 mg/kg of various DiR-labeled vectors. Images were taken at different times using IVIS Spectrum at 748 nm. Post-euthanasia, tissues were analyzed at 1, 6, and 12 h. The model was also used for pharmacokinetic studies with different DOX concentrations ($n = 3$). Blood samples were collected from the mice's orbital sinuses, and the DOX concentration was determined through high-performance liquid chromatography coupled with tandem mass spectrometry (HPLC−MS/MS).

2.12. Evaluating SPPexD antitumor efficacy

In the experiment utilizing a B16-F10 tumor-bearing mouse model, female C57BL/6 rodents were subjected to a subdermal injection of 1×10^6 B16-F10 melanoma cells on the right side of their torso. Seven days subsequent to this procedure, the subjects were assorted into ten distinct cohorts and commenced receiving bi-daily intravenous preparation (2 mg/kg of DOX). Tumor size and body weight of the mice in each group were monitored daily.

2.13. Assessing the anti-tumor efficacy of SPPexD combined with aPD-L1

The method was employed to establish the B16-F10 tumor model. Seven days post-tumor initiation, mice bearing B16-F10 tumors were randomly allocated to four groups and subjected to intravenous injections of normal saline, anti-PD-L1 antibody (aPD-L1), SPPexD, a combined therapy of SPPexD and aPD-L1 (administered at dosages of 2 mg/kg for DOX and 2 mg/kg for aPD-L1, respectively), preparation administered every two days, or aPD-L1 administered every four days. Daily observations were conducted to measure tumor size and monitor body weight.

2.14. Flow cytometry

The harvested neoplastic tissue underwent fine chopping before being enzymatically broken down to prepare a suspension of individual cells. Additionally, blood samples were collected from the mice *via* ocular extraction. Afterward, the cells underwent a staining process using fluorescently labeled antibodies that target CD3 (BioLegend), CD4 (BioLegend), Foxp3 (BioLegend), CD8 (BioLegend), CD44 (BioLegend), and CD62L (BioLegend). Each antibody was mixed at a dilution of 1:1000.

2.15. Statistical analysis

All data were calculated and assessed according to mean ± standard deviation (SD). Two tailed *t*-test or one-way analysis of variance (ANOVA) were applied to analyze the differences between comparative groups. The significant differences between the data were estimated at $P < 0.05$.

3. Results and discussion

3.1. Preparation and characterization of SPPexD

Exosomes were extracted from platelets using classical differential centrifugation. Transmission electron microscopy (TEM) (Fig. 1A) revealed that platelet exosome (Pex) exhibited a characteristic "disk-like" structure. The exosomes exhibited particle size of 82 ± 2.2 nm and zeta potential of −12.1 mV, consistent with the reported literature range of 30−150 nm[27]. Equivalent quantities of exosomes were incubated with DOX to prepare DOX-loaded platelet-derived exosomes (PexD). The DOX encapsulation was 21.83%. TEM analysis confirmed that the morphology of PexD remained unchanged. However, owing to the addition of positively charged DOX, the particle size increased to 90 ± 4.1 nm, and the surface potential shifted to −4.3 mV (Fig. 1B). The results demonstrated that loading DOX had no significant impact on the morphology, particle size, or surface potential of Pex.

PS serves as an apoptotic signal and is the primary recognition site for macrophages[28]. To mask PS, PexD was incubated with annexin V, resulting in the formation of PS-masked platelet-derived exosomes modified with annexin V (PPexD) (Fig. 1C and D). Flow cytometry revealed that phosphatidylserine (PS) fluorescence intensity on PPexD was significantly lower than that on normal Pex and similar to resting platelets. These findings suggested that PPexD could effectively mask PS on the surface of exosomes and thus has the potential to prevent macrophage recognition.

PPexD was incubated with MAL-PEOz-COOH at 37 °C overnight to obtain PS-shielded exosome spheres loaded with DOX (SPPexD) (Fig. 1F). Scanning electron microscopy (SEM) (Fig. 1E)−TEM (Supporting Information Fig. S1A), and particle size analysis confirmed the successful preparation of spherical SPPexD with an average size of 350 nm. After exposure to the tumor microenvironment (PBS, pH 6.5) for 1 h, SPPexD was analyzed *via* TEM (Fig. S1B and S1C) and particle size analysis (Fig. 1G). Our results indicated that the exosome spheres were pH

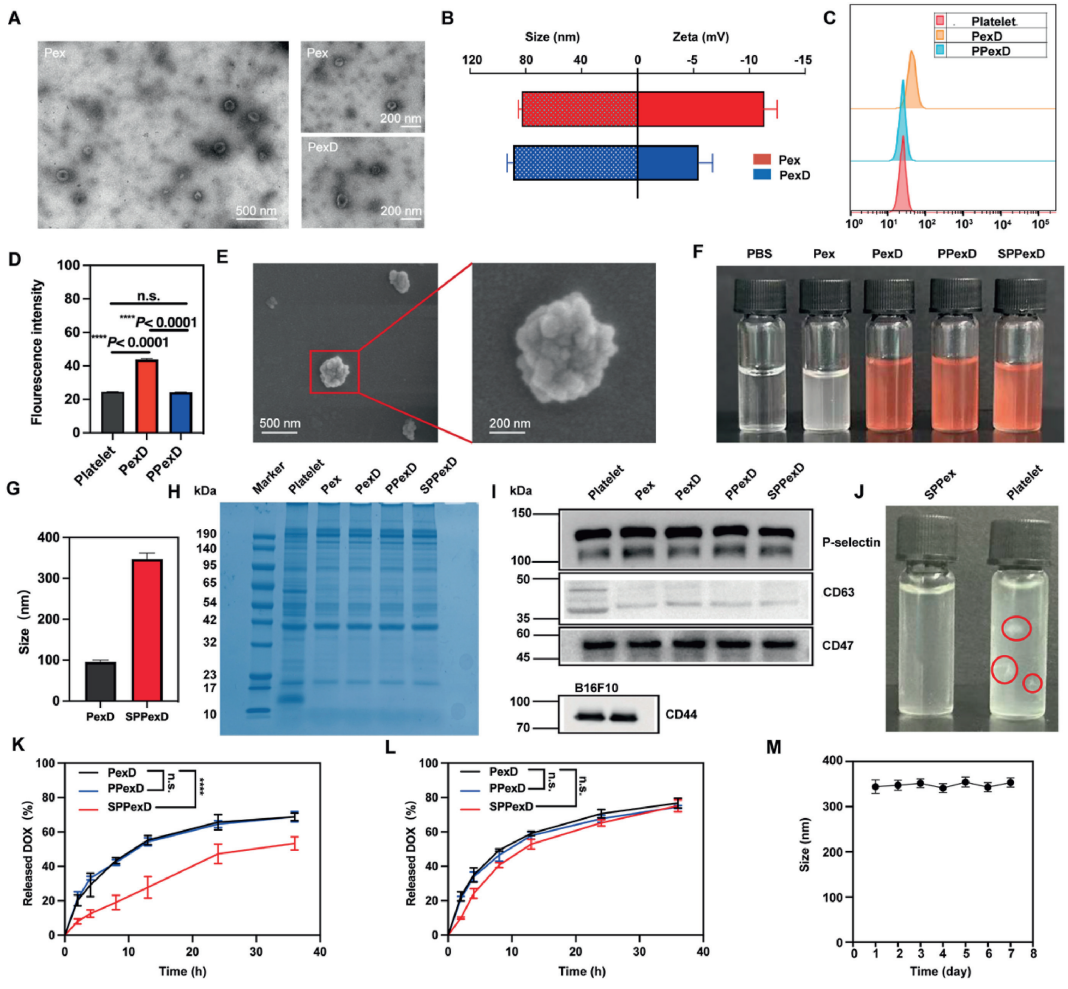

Figure 1 Characteristics of SPPexD. (A) TEM images of Pex and PexD are shown, with scale bars of 500 nm (left) and 200 nm (right). (B) Analysis of particle size and zeta potential for both Pex and PexD (n = 3). (C) Flow cytometry data evaluated the shielding of exosomal phosphatidylserine. (D) The relative quantification of phosphatidylserine was presented as the mean ± SD (n = 3). (E) Cryo-SEM images of SPPexD with scale bars of 500 nm (left) and 200 nm (right). (F) Image showed the appearance of the SPPexD preparation. (G) Particle size measurements comparing PexD and SPPexD (n = 3). (H) Protein analysis was conducted using SDS-PAGE. (I) Results of Western blot analysis. (J) Stability evaluation of SPPex and platelets. (K) Profiles of DOX release from different formulations in PBS at pH 7.4 (n = 3). (L) DOX release profiles in PBS at pH 6.5 for different formulations (n = 3). (M) Changes in particle size of SPPex after one week of storage at 4 °C (n = 3).

sensitive. The hydrazone bonds connecting the exosomes become protonated in the acidic tumor microenvironment, causing them to disintegrate into uniform-sized single exosomes.

SDS-PAGE analysis revealed that SPPexD retained unique proteins expressed on platelet and Pex (Fig. 1H). Western blotting confirmed the expression of essential proteins on platelet, Pex, and SPPexD (Fig. 1I, Supporting Information Fig. S2). Notably, the exosome biomarker CD63, CD9, TSG101 were expressed on SPPexD, as well as on purified small extracellular vesicles obtained by differential ultracentrifugation. The cell adhesion molecule P-selectin, which could bind to CD44 expressed on B16-F10 cells, was identified on SPPexD. Similarly, CD47, which interacts with Sirpα on macrophage surfaces to transmit inhibitory signals and prevent phagocytosis, was also detected on SPPexD. These proteins coexisted on platelet, Pex, PPexD, and SPPexD, indicating that functional proteins were retained on SPPexD during the modification process.

We next explored the cumulative release of DOX. Under physiological conditions (pH 7.4) (Fig. 1K), the cumulative release of DOX from PexD reached 45.3% at 8 h and increased to 60.8% at 24 h. PPexD exhibits similar release behavior to PexD. The results indicated that annexin V modification does not significantly alter DOX release kinetics. However, SPPexD showed a reduced release rate with a cumulative release of 20.2% of DOX at 8 h and a cumulative release of 46.2% at 24 h. This phenomenon was likely due to the spherical structure of exosomes, which created an additional diffusion barrier that impeded the release of DOX.

In contrast, under the acidic conditions (pH 6.5) (Fig. 1L), the PEOz hydrazone bond within SPPexD was protonated, resulting in the disintegration of the spheres into individual exosomes. Therefore, under these conditions, the DOX release profile of SPPexD was similar to that of PexD, showing a comparable cumulative release profile. Preparation and storage stability are crucial aspects of drug development, drug production, and quality control. Consequently, we investigated the stability of PPex (PS-masked platelet-derived exosomes) aggregates (SPPex). By utilizing appearance photography and particle size measurement (Fig. 1J and M), we found that SPPex could be stably stored for 1 week at 4 °C. In comparison, platelet aggregation was observed after one day of storage at 4 °C. We also found no change in the particle size of SPPex in rat plasma after storage at 37 °C for one week (Supporting Information Fig. S3). These findings demonstrated that, in contrast to platelet, SPPex had good stability, thereby ensuring drug efficacy and safety.

3.2. Ex vitro evaluation of SPPexD

Due to the high quantity of macrophages in the liver and spleen, exosomes tend to predominantly accumulate in these organs[29]. To assess the antiphagocytic ability of SPPex, we incubated DIR-labeled Pex, PPex, platelet, and SPPex with macrophages for 1 h. As shown in Fig. 2A and Supporting Information Fig. S6A, the DIR-labeled platelet group exhibited the lowest macrophage uptake, potentially due to the low surface PS content and high CD47 expression in the resting platelets. Compared with the single exosome group, both the PPex and SPPex groups demonstrated enhanced antiphagocytic abilities. Significantly, due to the aggregate of exosomes, SPPex exhibited the strongest resistance to phagocytosis. This effect is credited to the shielding of PS and the increased number of CD47 sites (recognition sites for macrophage Sirpα), provides a basis for the long blood circulation of SPPexD.

To assess the cell adhesion properties of the exosome spheres, B16-F10 cells were incubated with fluorescently labeled Pex, PPex, SPPex, or platelets at 4 °C for 1 h. As shown in Fig. 2B and Supporting Information Fig. S4, Pex and PPex exhibited comparable fluorescence intensities, suggesting that the modification of the exosome surface with annexin V did not alter the adhesion of Pex to tumor cells. However, DIR-labeled SPPex and platelets presented higher fluorescence intensities than Pex in B16-F10 cells, showing that the adherence to tumor cells improved by exosome aggregation into spheres. The increased adherence was ascribed to the surface of the exosome spheres' increased P-selectin, a recognition site for CD44, exposure.

To examine the ability of SPPexD to internalize DOX into cells, we co-incubated B16-F10 cells with different DOX-containing formulations at 37 °C for 0.5 and 2 h (Supporting Information Fig. S5). At the same time points, SPPexD exhibited the highest cellular uptake efficiency. This was attributed to the fact that SPPexD expressed higher levels of P-selectin (a recognition site for CD44) than did PexD and PPexD, allowing it to rapidly bind to B16-F10 cells. This finding suggested that the elevation of cellular uptake was a consequence of increased cell adhesion. Flow cytometry was used to quantitatively evaluate DOX uptake by B16-F10 cells in different solutions. As shown in Fig. 2C and D, SPPexD exhibited a superior ability to enhance DOX uptake by B16-F10 cells when compared to DOX-loaded platelets. Although platelets adhered better to B16-F10 cells than SPPexD did, the B16-F10 cells could not effectively internalize the larger platelets. DOX could only passively diffuse into cells from the platelets. In contrast, SPPexD could not only effectively adhere to tumor cells but could also be actively internalized by B16-F10 cells.

The cytotoxicity of different DOX-containing formulations was assessed *in vitro* using the MTT assay. As shown in Fig. 2E, the IC_{50} values for SPPexD, PexD, and DOX-loaded platelets were calculated as 0.094, 0.184, and 0.307 μg/mL, respectively. The enhanced cellular absorption of DOX in the SPPexD group allowed SPPexD to show a significantly higher cytotoxic effect on B16-F10 cells than other formulations.

Chemotherapeutic drugs, such as DOX, can induce immunogenic cell death (ICD) in tumor cells, thereby triggering the maturation of dendritic cells (DCs)[11]. We investigated the release of HMGB1 and ATP in B16-F10 cancer cells following treatment with SPPexD, PPexD, DOX-loaded platelet, PexD, and free DOX (Fig. 2F and G). The results demonstrated that, compared with the other treatments, SPPexD led to greater release of HMGB1 and ATP, which are pivotal signaling molecules involved in ICD. Moreover, co-culturing bone marrow-derived dendritic cells (BMDCs) with tumor cells treated with SPPexD led to increased expression of the costimulatory molecules CD80 and CD86, which served as indicators of dendritic cell maturation. These findings suggested that SPPexD-induced ICD effectively promoted DC maturation (Fig. 2H, Fig. S6B).

To further assess the drug delivery potential of SPPexD and related drugs, we employed multicellular spheroids (MCSs) as an *in vitro* three-dimensional (3D) model that mimics B16−F10 tumor tissue. This model was used to evaluate SPPexD permeability. To mitigate the interference of DOX fluorescence, we utilized DIR-labeled Pex, PPex, platelet, and SPPex and coincubated them with MCSs at a pH of 6.5. As depicted in Supporting Information Fig. S7, at 1 h, DIR-labeled platelets (red) and SPPex with strong adhesion abilities were efficiently adsorbed on the exterior of the MCSs. Owing to their smaller particle size, PPex and Pex could be detected inside the MCSs, albeit at a lower intensity. After 6 h, the

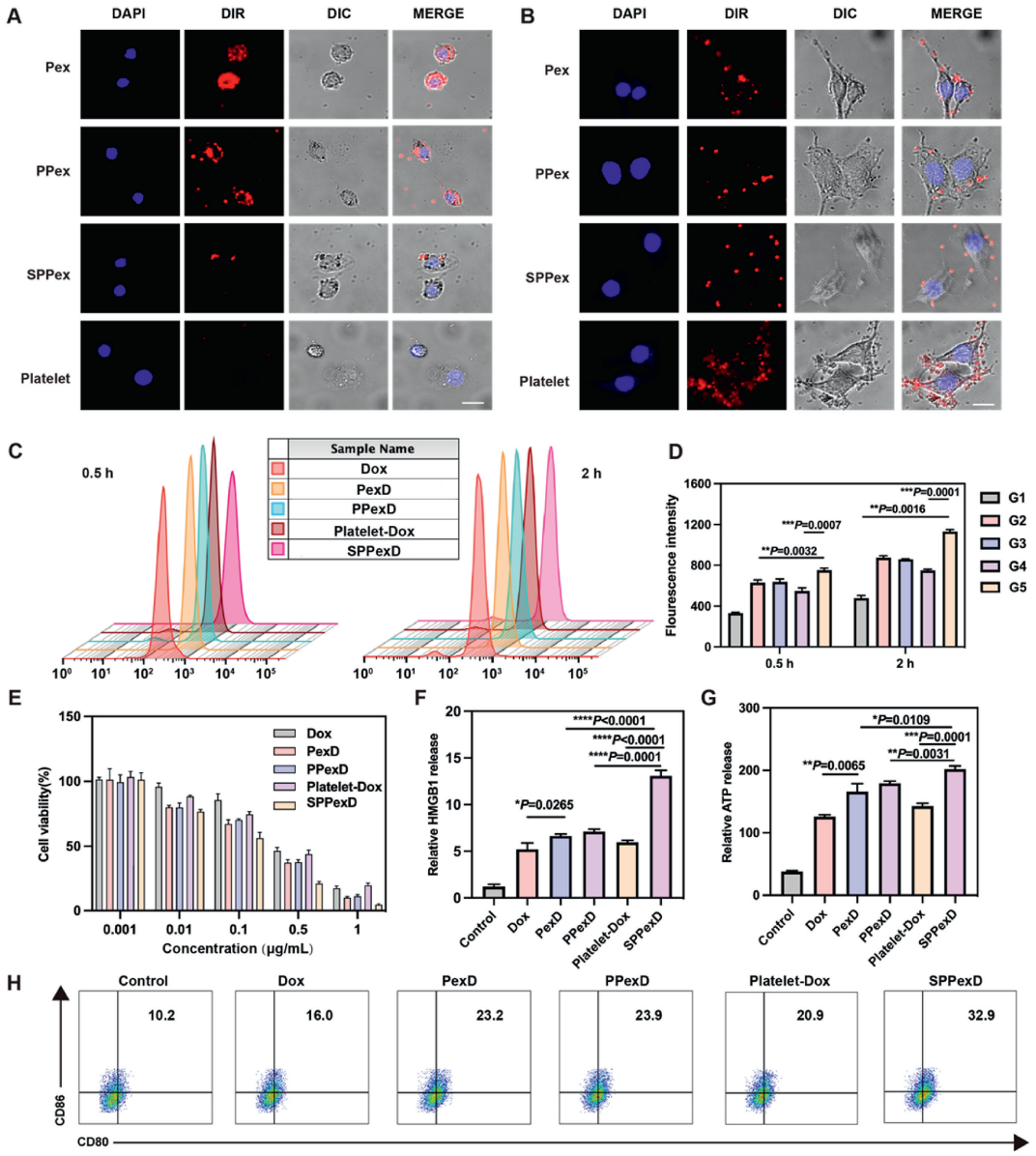

Figure 2 *In vitro* evaluation of SPPexD. (A) Various DiR-labeled vectors were incubated with RAW264.7 macrophages at 37 °C for 1 h to evaluate their interaction. Scale bar: 10 μm. (B) The adhesion capacity was assessed by incubating different DiR-labeled vectors with B16-F10 cells at 4 °C for 1 h. Scale bar: 10 μm. (C) Flow cytometry was used to analyze the cellular uptake by B16-F10 cells after incubation with the respective formulations for 0.5 and 2 h. (D) Quantitative analysis of cellular uptake was performed ($n = 3$). (G1: Dox G2: PexD G3: PPexD G4: platelet-Dox G5: SPPexD). (E) The cytotoxicity of various DOX-containing formulations was evaluated on B16-F10 cells ($n = 3$). (F) HMGB1 release following 24 h of treatment of B16-F10 cells with various DOX-containing formulations ($n = 3$). (G) ATP release after 24 h of treating B16-F10 cells with the same formulations ($n = 3$). (H) Maturation of dendritic cells induced by various formulations ($n = 3$).

fluorescence intensity of SPPex within the MCSs was comparable to that of PPex and Pex, whereas the platelets remained primarily at the periphery of the MCSs. This was attributed to the breakdown of the adsorbed SPPex into individual exosomes at low pH and the subsequent spread of the SPPex uniformly among the MCSs. Notably, although platelets clearly adhered to MCSs at 1 h, their permeability in the tumor spheroids was the lowest due to their large size and the varying sizes of activated-derived vesicles. These findings suggested that, compared with platelets, SPPexD exhibit a significantly increased ability to penetrate MCSs, paving the way for subsequent *ex vivo* tumor penetration studies.

3.3. *In vivo eradication of CTCs in the circulatory system*

Originally from solid tumors, circulating tumor cells (CTCs) separate from the main tumor mass and enter the bloodstream. In cancer patients, these CTCs may reside as single cells or cell clusters within the blood, showing a considerable potential for metastasis[30-32]. To evaluate the ability of SPPexD to capture CTCs, we conducted an experiment in which mice were intravenously injected with saline, DOX solution, PexD, PPexD, DOX-loaded platelet, or SPPexD (40 μg DOX per mouse). To simulate the behavior of CTCs *in vivo*, a suspension of 2×10^6 B16-F10 tumor

cells in single-cell form was administered into C57BL/6 mice through the tail vein.

As illustrated in Supporting Information Fig. S8, the lungs of mice treated with SPPexD displayed nearly no metastatic nodules, highlighting the superior efficiency of SPPexD in capturing CTCs. While the PexD and DOX-loaded platelet groups also showed some anti-metastatic effects, their efficacy was notably lower compared to SPPexD.

Compared to other treatment groups, SPPexD demonstrated superior efficacy in inhibiting tumor metastasis, primarily due to its multiple advantages. The increased antiphagocytic capability enabled effective capture of CTCs prior to immune clearance, the favorable adhesion properties facilitated close binding to CTCs; and their smaller particle size compared with that of platelets, allowed for smoother traversal of cell barriers in the body and deeper penetration. Additionally, within the bloodstream, SPPexD exhibited higher levels of P-selectin compared to exosomes, enabling more effective binding to CD44 on CTCs and thereby enhancing its capacity to capture CTCs. Following successful capture of CTCs, the DOX encapsulated within SPPexD directly eradicated tumor cells, mitigating the risk of metastasis.

3.4. *SPPexD triggers strong immune response*

Next, various formulations (PBS, Pex, PPex, SPPex, platelet, DOX, PexD, PPexD, DOX-loaded platelets and SPPexD) were administered to tumor-bearing C57BL/6 mice *via* tail vein injection. After 18 days of treatment, tumor and blood samples were collected from the mice, and immune cells were isolated and analyzed using flow cytometry (Fig. 3A). The saline and vector groups showed similar results, with no significant immune effects detected. In contrast, treatment with the DOX-containing formulation led to an increase in tumor-infiltrating cytotoxic T lymphocytes (Fig. 3B and E) and memory T cells in the blood (Fig. 3D and G). Simultaneously, there was a reduction in tumor-associated immunosuppressive T cells (Fig. 3C and F). These findings indicated that DOX-encapsulated formulations can activate T-cell-mediated immune responses. SPPexD could elicit a more robust T cell immune response than other formulations, as evidenced by a 3.16-fold increase in the number of tumor-infiltrating cytotoxic T lymphocytes, a 1.98-fold increase in the proportion of memory T cells in the blood, and a 1.79-fold decrease in the number of tumor regulatory T cells, all

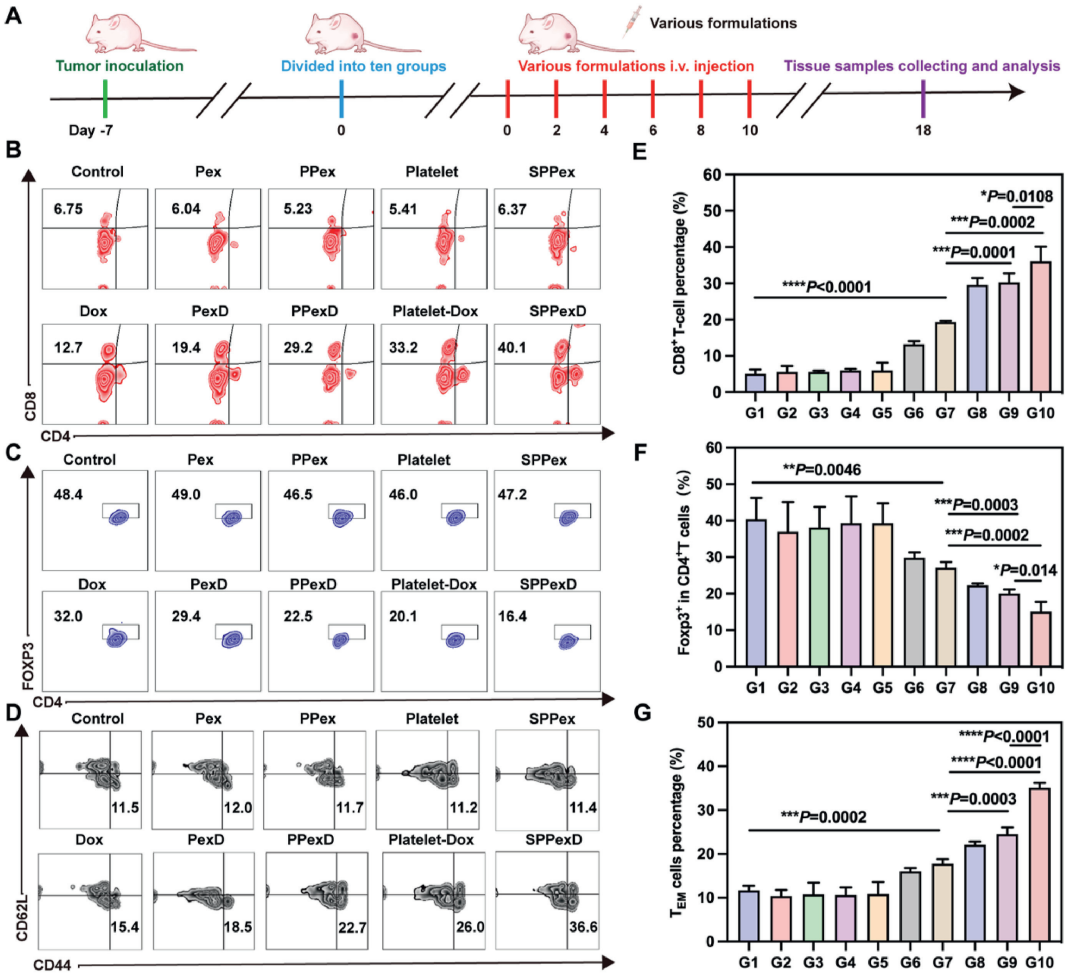

Figure 3 The analysis of immune cells in blood and tumor samples collected from mice 18 days after treatment with different preparations. (A) Schematic representation of the treatment regimen: tumor-bearing mice were administered various agents *via* tail vein injection (DOX 2 mg/kg, every 2 days). (B) Representative images showing $CD8^+$ T cells. (C) Representative images displaying $Foxp3^+$ T cells. (D) Representative images illustrating effector memory T cells. (E) Quantitative analysis of $CD8^+$ T cell populations ($n = 4$). (F) Quantitative analysis of $Foxp3^+$ T cell populations ($n = 4$). (G) Quantitative analysis of effector memory T cell populations ($n = 4$). (E–G): G1 (Control), G2 (Pex), G3 (PPex), G4 (platelet), G5 (SPPex), G6 (DOX), G7 (PexD), G8 (PPexD), G9 (platelet-DOX), G10 (SPPexD).

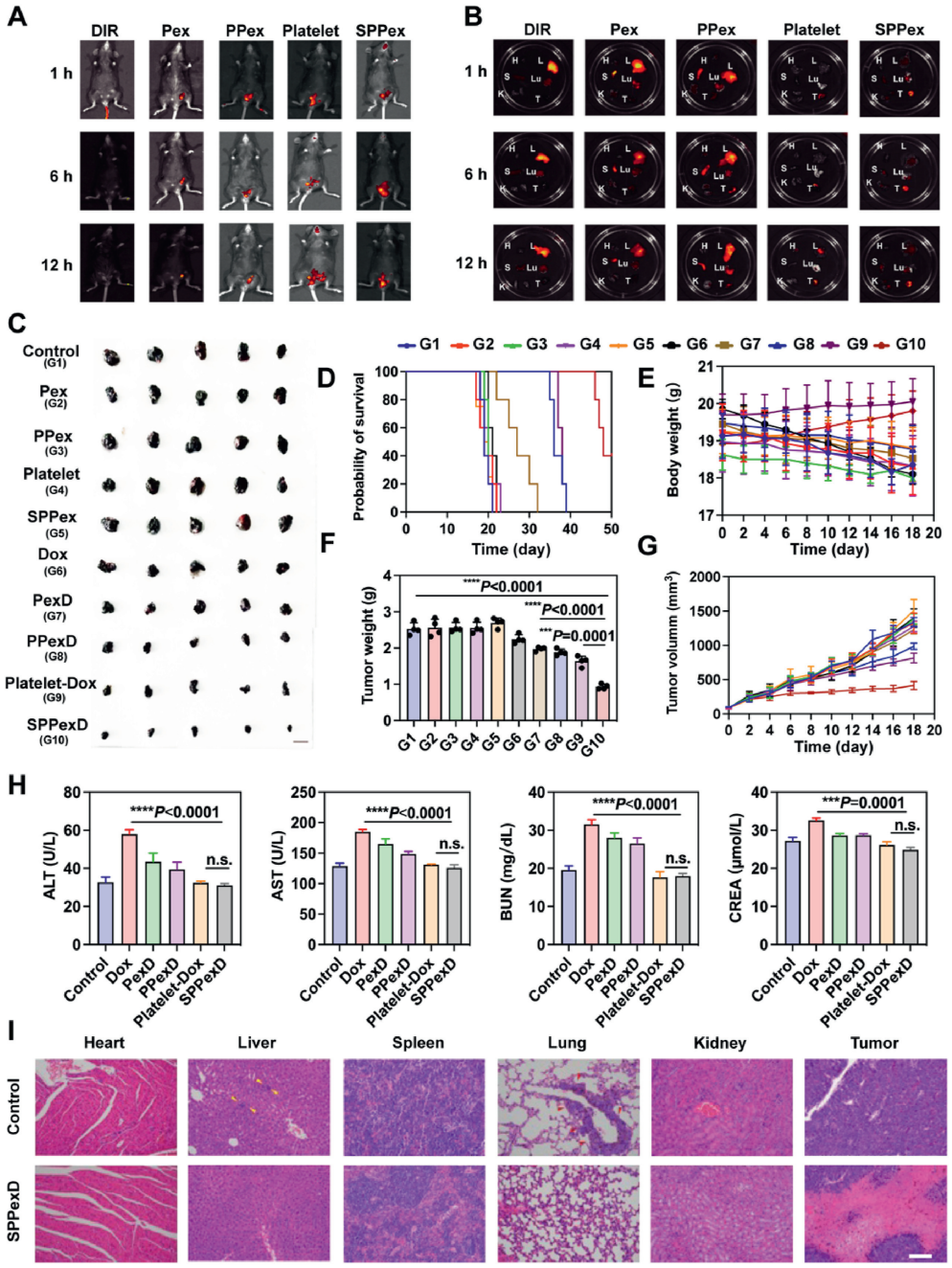

Figure 4 SPPexD demonstrates anti-Phagocytic and tumor targeting abilities. (A) *In vivo* fluorescence imaging of B16-F10 tumor-bearing mice at 1, 6, and 12 h post-intravenous injection of free DiR solution, DiR-labeled Pex, PPex, platelet-mimetics, and SPPex. (B) *Ex vivo* fluorescence imaging of major tissues collected at 1, 6, and 12 h post-injection with the preparations. SPPexD's tumor inhibitory effects. (C) Post-treatment tumor images from mice in each group. (D) Survival rates of mice across various treatment groups ($n = 5$). (E) Body weight changes in mice from different treatment groups ($n = 4$). (F) Tumor weight quantification in mice after treatment ($n = 4$). (G) Tumor growth curves in mice from different groups during the treatment period ($n = 6$). (H) Assessment of liver and kidney function in mice treated with DOX-containing preparations ($n = 3$). (I) H&E staining of major mouse organs. Scale bar: 1 mm $^*P < 0.05$, $^{**}P < 0.01$, $^{***}P < 0.001$, $^{****}P < 0.0001$.

compared to PexD. Since SPPexD could effectively deliver DOX into tumors, the released DOX could trigger ICD of tumor cells, thereby functioning as a "tumor vaccine" to rejuvenate nonfunctional T cells. Taken together, these data implied that the potent antitumor capacity of SPPexD may be attributed to their efficient drug delivery abilities, which increased DC phagocytosis, DC maturation, and $CD8^+$ T-cell activation, thereby bolstering antitumor immunity.

3.5. In vivo antitumor efficacy of SPPexD in B16-F10 tumor-bearing mice

To evaluate the therapeutic efficacy of our approach, we established a melanoma mouse model. First, pharmacokinetic studies were performed to evaluate the antiphagocytic properties of SPPexD (intravenous injection of DOX, PexD, PPexD, or SPPexD). As shown in Supporting Information Fig. S9A, DOX

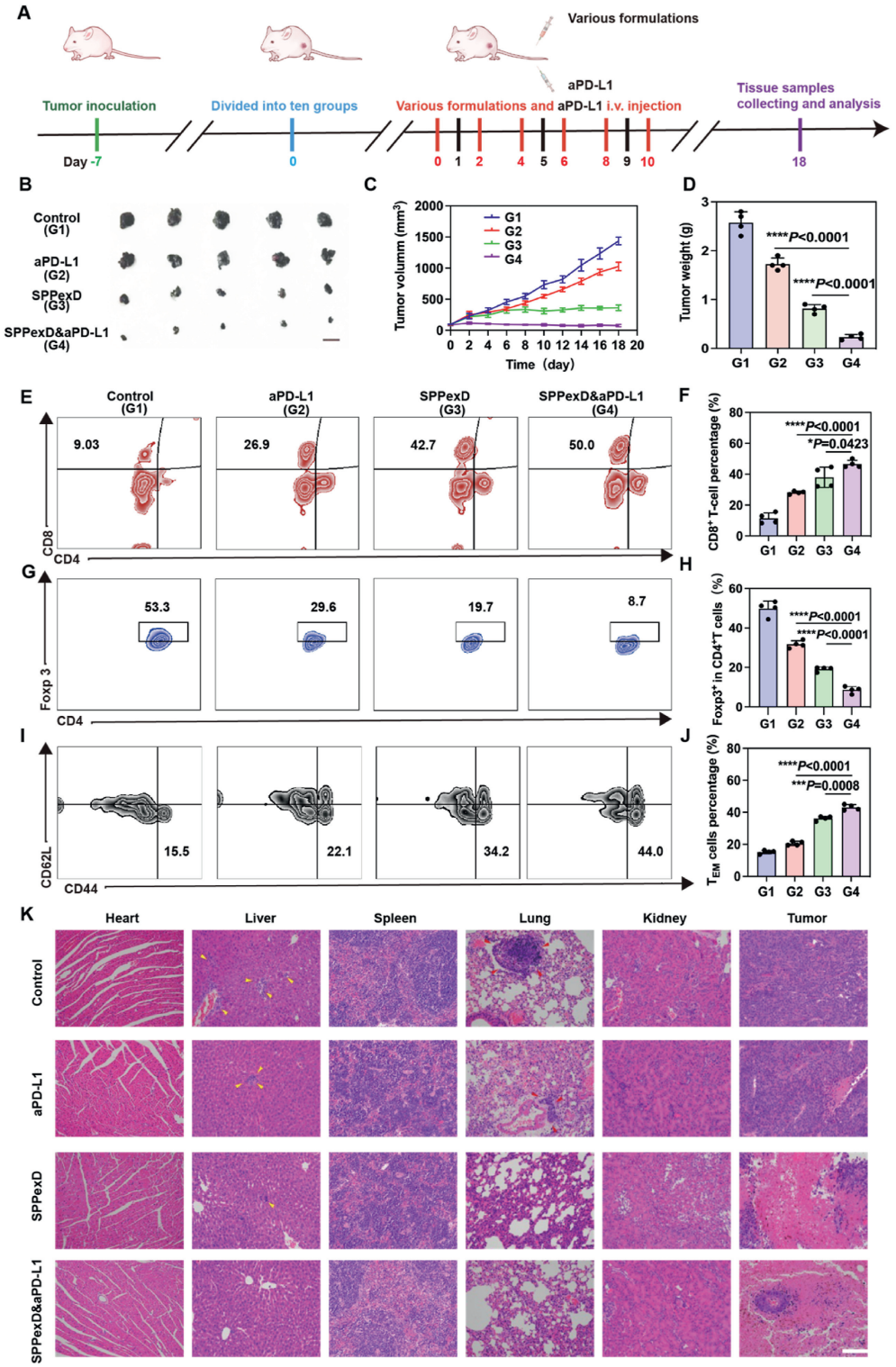

Figure 5 SPPexD significantly enhances the anti-tumor efficacy of anti-PD-L1 antibodies. (A) Schematic timeline depicting the administration of PBS, four blank vectors, DOX, PexD, PPexD, platelet-DOX, and SPPexD (2 mg/kg, once every 2 days) *via* tail vein injection. Additionally, anti-PD-L1 antibody was administered *via* tail vein injection at a dose of 2 mg/kg every 4 days for a total of three injections. (B) Photographs of mouse tumors following different treatment regimens. (C) Growth curves of mouse tumors after undergoing various treatments ($n = 6$). (D) Quantitative analysis of mouse tumor weights post-treatment ($n = 4$). (E) Representative images of $CD8^+$ T cells across various formulation groups post-treatment. (G) Representative images of $Foxp3^+$ T cells in different formulation groups following treatment. (I) Representative images of effector memory T cells observed in different formulation groups after treatment. (F, H, J) Quantitative analysis corresponding to the data shown in (D, E, G) ($n = 4$). (K) H&E staining of major organs from various treatment groups. Scale bar: 1 mm.

solution was metabolized within less than 10 min after injection, while the half-life of DOX in PexD was 0.46 h. The half-life of DOX in PPexD, in which PS was shielded, reached 1.21 h, which was 2.6 times greater than that of DOX in PexD, indicating that PS masking can prolong the circulation time of exosomes in the blood. The half-life of DOX in SPPexD was determined to be 2.41 h, which is 5.24 times longer than that in PexD and 1.99 times longer than that in PPexD, significantly prolonging the blood circulation time of DOX. Subsequently, biodistribution studies were conducted using DIR-labeled formulations (DIR, DIR-labeled Pex, DIR-labeled PPex, DIR-labeled platelet, and DIR-labeled SPPex) in the same animal model (Fig. 4A and B). Notably, SPPex accumulation peaked in the tumor 6 h after injection, with the number of SPPex being 2.01- and 1.82-fold greater than that of Pex and PPex, respectively (Fig. S9B). In addition, compared with Pex, which were taken up by macrophage-rich organs such as the liver and spleen, SPPex exhibited reduced aggregation, similar to platelets. In summary, owing to the masking of phagocytic signals on SPPex and the enhanced targeting ability of P-selectin, SPPex had a long circulation time, high targeting ability similar to that of platelets, and a good ability to penetrate tumor sites.

In addition, the antitumor activity of SPPexD was evaluated in subcutaneous B16-F10 tumors, and the results revealed that the tumor inhibition rate of the SPPexD was significantly greater than that of PexD and DOX-loaded platelets (Fig. 4C−F, G). Notably, following treatment with SPPexD, the tumors in the mice progressively regressed (Supporting Information Fig. S10), and the mice's survival time was considerably increased (Fig. 4D), forty percent of the mice survived beyond 50 days. As shown in Supporting Information Figs. S11 and S12, we performed DOX tumor penetration experiments. Compared with the other formulation groups, the SPPexD group had better tumor penetration ability. Additionally, an evaluation of systemic toxicity revealed only a slight reduction in body weight among the different treatment groups, with the exception of those in the SPPexD and platelet-DOX (Fig. 4E). This could suggest the presence of systemic toxicity. Conversely, the weights of mice in both the SPPexD and platelet-DOX assemblies did not vary. The HE staining results showed that the major organs in the SPPexD treatment group exhibited no significant signs of tumor metastasis (Fig. 4I and Supporting Information Fig. S13). DOX, a classic effective anthracycline antibiotic with significant antitumor effects, is widely used to treat various malignancies. However, the therapeutic application of DOX is constrained due to its liver and kidney toxicities[33]. The hepatotoxicity assessment (Fig. 4H) indicated elevated levels of alanine aminotransferase (ALT), aspartate aminotransferase (AST), and blood urea nitrogen (BUN) in mice treated with DOX, PexD, and PPexD compared to the saline group. In contrast, the platelet-DOX and SPPexD treatment groups showed ALT, AST, and BUN levels comparable to those observed in the saline group. These results suggested that platelet-DOX and SPPexD possessed a favorable safety profile, attributed to the prolonged blood circulation time and efficient targeting capability of SPPexD. In conclusion, SPPexD, as a novel drug delivery system, effectively delivered DOX to tumor sites while significantly reducing hepatotoxicity and renal toxicity, potentially representing a new clinical treatment option.

3.6. SPPexD markedly boost antitumor efficiency of anti-PD-L1 antibody

We treated tumors with SPPexD combined with anti-PD-L1 antibodies to further assess the ability of SPPexD to enhance anticancer effects. B16-F10 tumor-bearing mice were injected with PBS or SPPexD *via* the tail vein, followed by either intravenous injection of anti-PD-1 antibodies or no further treatment (Fig. 5A). As expected, compared with PBS, anti-PD-L1 antibody treatment alone caused weak tumor inhibition. SPPexD significantly inhibited tumor growth (Fig. 5B−D and Supporting Information Fig. S14A). However, SPPexD combined with anti-PD-L1 treatment had the most pronounced tumor-inhibiting effect, with 60% of the mice surviving up to 50 days after tumor inoculation (Fig. S14B) and no change in body weight (Fig. S14C).

The immune responses elicited by each treatment group were subsequently analyzed. Among all groups, the SPPexD&anti-PD-L1 combination demonstrated the highest proportion of $CD8^+$ T cells within the tumor microenvironment and memory T cells circulating in the blood, while the percentage of $Foxp3^+$ T cells at the tumor site was the lowest (Fig. 5E−J). Compared with that in the saline group, spleen tissue morphology in the SPPexD&anti-PD-L1 group was normal, and H&E staining (Fig. 5K) revealed that, after the combination treatment, there was essentially no tumor metastasis to the main organs. The above results demonstrated that SPPexD&anti-PD-L1 treatment not only activated the immune system but also markedly reduced the progression of tumors. These findings suggested that SPPexD substantially augmented the efficacy of anti-PD-L1 therapy.

4. Conclusions

In summary, we have developed a novel formulation of exosome spheres for the delivery of chemotherapy drugs to treat tumors. Our aim was to increase the efficiency of chemotherapy drug delivery and regulate tumor immunity. These exosome spheres were composed of PS-shielded platelet-derived exosome aggregates, which feature increased recognition sites for CD44 (mediated by P-selectin) and macrophage SIRP-α (binding to CD47) on tumor cells. These features allow the exosome spheres to effectively block apoptosis signals, thereby significantly improving the antiphagocytosis and targeting capabilities of the exosomes. In the B16-F10 tumor model, SPPexD robustly triggered ICD, stimulating T-cell activation and enhancing the efficacy of immunotherapy. Due to their targeted delivery capability and extended circulation time in the bloodstream, SPPexD demonstrated minimal toxicity to healthy tissues and effectively mitigated the adverse effects of chemotherapy drugs on the liver and kidneys. When combined with an anti-PD-L1 monoclonal antibody, SPPexD effectively inhibited tumor growth, overcoming the challenge of the low response rate to ICD therapy to a great extent. The proposed formulation represents a promising adjuvant for various monoclonal antibodies (mAbs), aiming to improve clinical outcomes by specifically targeting and killing cancer cells while enhancing the efficacy of ICB therapy.

Acknowledgements

We are grateful for the financial support from National Key R&D Program of China (No. 2022YFE0111600), National Natural

Science Foundation of China (No. 82273874), Liaoning Revitalization Talents Program (No. XLYC22202019, China).

Author contributions

Jian Zhao, Xinyan Lv, Hao Ye, and Jin Sun conceived the project. Jian Zhao, Qi Lu, Kaiyuan Wang, Xiaoyuan Fan, Lili Du, Xinyan Lv, Fengxiang Liu, and Fei Sun performed the experiments. Jian Zhao, Xinyan Lv, Hao Ye, Kaiyuan Wang, and Jin Sun analyzed the results. Zhonggui He provided useful suggestions for this work. Jian Zhao, Hao Ye, and Jin Sun wrote the manuscript.

Conflicts of interest

The authors declare no conflict of interest.

Appendix A. Supporting information

Supporting information to this article can be found online at https://doi.org/10.1016/j.apsb.2025.04.013.

References

1. Holder AM, Dedeilia A, Sierra-Davidson K, Cohen S, Liu D, Parikh A, et al. Defining clinically useful biomarkers of immune checkpoint inhibitors in solid tumours. *Nat Rev Cancer* 2024;**24**:498−512.
2. Wang DR, Wu XL, Sun YL. Therapeutic targets and biomarkers of tumor immunotherapy: response *versus* non-response. *Signal Transduct Targeted Ther* 2022;**7**:331.
3. Kirchhammer N, Trefny MP, Auf der Maur P, Läubli H, Zippelius A. Combination cancer immunotherapies: emerging treatment strategies adapted to the tumor microenvironment. *Sci Transl Med* 2022;**14**: eabo3605.
4. Huang AC, Zappasodi R. A decade of checkpoint blockade immunotherapy in melanoma: understanding the molecular basis for immune sensitivity and resistance. *Nat Immunol* 2022;**23**:660−70.
5. Guan X, Hu R, Choi Y, Srivats S, Nabet BY, Silva J, et al. Anti-TIGIT antibody improves PD-L1 blockade through myeloid and Treg cells. *Nature* 2024;**627**:646−55.
6. Quandt Z, Jacob S, Fadlullah MZH, Wu C, Wu C, Huppert L, et al. Phase II trial of pembrolizumab, ipilimumab, and aspirin in melanoma: clinical outcomes and translational predictors of response. *BJC Rep* 2024;**2**:46.
7. Blum SM, Zlotoff DA, Smith NP, Kernin IJ, Ramesh S, Zubiri L, et al. Immune responses in checkpoint myocarditis across heart, blood, and tumor. *bioRxiv* 2023. Available from: https://doi.org/10.1101/2023.09.15.557794.
8. Ye H, Wang K, Zhao J, Lu Q, Wang M, Sun B, et al. *In situ* sprayed nanovaccine suppressing exosomal PD-L1 by Golgi apparatus disorganization for postsurgical melanoma immunotherapy. *ACS Nano* 2023;**17**:10637−50.
9. Sun Q, Hong Z, Zhang C, Wang L, Han Z, Ma D. Immune checkpoint therapy for solid tumours: clinical dilemmas and future trends. *Signal Transduct Targeted Ther* 2023;**8**:320.
10. Patel SA, Minn AJ. Combination cancer therapy with immune checkpoint blockade: mechanisms and strategies. *Immunity* 2018;**48**:417−33.
11. Zhao J, Ye H, Lu Q, Wang K, Chen X, Song J, et al. Inhibition of postsurgery tumour recurrence *via* a sprayable chemo-immunotherapy gel releasing PD-L1 antibody and platelet-derived small EVs. *J Nanobiotechnol* 2022;**20**:62.
12. Lyu C, Sun H, Sun Z, Liu Y, Wang Q. Roles of exosomes in immunotherapy for solid cancers. *Cell Death Dis* 2024;**15**:106.
13. Kim TK, Vandsemb EN, Herbst RS, Chen L. Adaptive immune resistance at the tumour site: mechanisms and therapeutic opportunities. *Nat Rev Drug Discov* 2022;**21**:529−40.
14. Kumar MA, Baba SK, Sadida HQ, Marzooqi SA, Jerobin J, Altemani FH, et al. Extracellular vesicles as tools and targets in therapy for diseases. *Signal Transduct Targeted Ther* 2024;**9**:27.
15. Lu P, Ruan D, Huang M, Tian M, Zhu K, Gan Z, et al. Harnessing the potential of hydrogels for advanced therapeutic applications: current achievements and future directions. *Signal Transduct Targeted Ther* 2024;**9**:166.
16. Lu Q, Liu T, Han Z, Zhao J, Fan X, Wang H, et al. Revolutionizing cancer treatment: the power of cell-based drug delivery systems. *J Control Release* 2023;**361**:604−20.
17. Ravichandran KS. Beginnings of a good apoptotic meal: the find-me and eat-me signaling pathways. *Immunity* 2011;**35**:445−55.
18. Birge RB, Boeltz S, Kumar S, Carlson J, Wanderley J, Calianese D, et al. Phosphatidylserine is a global immunosuppressive signal in efferocytosis, infectious disease, and cancer. *Cell Death Differ* 2016; **23**:962−78.
19. Osorio JC, Smith P, Knorr DA, Ravetch JV. The antitumor activities of anti-CD47 antibodies require Fc-FcγR interactions. *Cancer Cell* 2023; **41**:2051-65.e6.
20. Feng Q, Ma X, Cheng K, Liu G, Li Y, Yue Y, et al. Engineered bacterial outer membrane vesicles as controllable two-way adaptors to activate macrophage phagocytosis for improved tumor immunotherapy. *Adv Mater* 2022;**34**:e2206200.
21. Zhang N, Ping W, Suo M, Zhang Z, Zhang W, Zhang T, et al. Biomimetic nanosystem loading aggregation-induced emission luminogens and SO_2 prodrug for inhibiting insufficient photothermal therapy-induced breast cancer recurrence and metastasis. *Adv Sci (Weinh)* 2024;**11**:e2405575.
22. Bala Tannan N, Manzari MT, Herviou L, Da Silva Ferreira M, Hagen C, Kiguchi H, et al. Tumor-targeted nanoparticles improve the therapeutic index of BCL2 and MCL1 dual inhibition. *Blood* 2021; **137**:2057−69.
23. Liu H, Jiang S, Li M, Lei S, Wu J, He T, et al. Dual enzyme-driven cascade reactions modulate immunosuppressive tumor microenvironment for catalytic therapy and immune activation. *ACS Nano* 2024;**18**: 30345−59.
24. Chen L, Yin Q, Zhang H, Zhang J, Yang G, Weng L, et al. Protecting against postsurgery oral cancer recurrence with an implantable hydrogel vaccine for *in situ* photoimmunotherapy. *Adv Sci (Weinh)* 2024:e2309053.
25. Guo Y, Li Y, Zhang M, Ma R, Wang Y, Weng X, et al. Polymeric nanocarrier *via* metabolism regulation mediates immunogenic cell death with spatiotemporal orchestration for cancer immunotherapy. *Nat Commun* 2024;**15**:8586.
26. Xu KF, Wu SY, Wang Z, Guo Y, Zhu YX, Li C, et al. Hyperbaric oxygen enhances tumor penetration and accumulation of engineered bacteria for synergistic photothermal immunotherapy. *Nat Commun* 2024;**15**:5147.
27. Kalluri R. The biology and function of extracellular vesicles in immune response and immunity. *Immunity* 2024;**57**:1752−68.
28. Groß R, Reßin H, von Maltitz P, Albers D, Schneider L, Bley H, et al. Phosphatidylserine-exposing extracellular vesicles in body fluids are an innate defence against apoptotic mimicry viral pathogens. *Nat Microbiol* 2024;**9**:905−21.
29. Isaac R, Reis FCG, Ying W, Olefsky JM. Exosomes as mediators of intercellular crosstalk in metabolism. *Cell Metab* 2021;**33**:1744−62.
30. Li W, Zhang X, Yang Y, Lin J, Zhou K, Sun R, et al. Circulating tumor cells are a good predictor of tumor recurrence in clinical patients with gastric cancer. *Sci Rep* 2024;**14**:12758.
31. Chen Y, Lin M, Ye D, Wang S, Zuo X, Li M. Functionalized tetrahedral DNA frameworks for the capture of circulating tumor cells. *Nat Protoc* 2024;**19**:985−1014.
32. Yang C, Wang X, To KKW, Cui C, Luo M, Wu S, et al. Circulating tumor cells shielded with extracellular vesicle-derived CD45 evade T cell attack to enable metastasis. *Signal Transduct Targeted Ther* 2024; **9**:84.
33. Fralish Z, Chen A, Khan S, Zhou P, Reker D. The landscape of small-molecule prodrugs. *Nat Rev Drug Discov* 2024;**23**:365−80.